ELSEVIER

Journal of Alloys and Compounds 441 (2007) 146–151

Journal of ALLOYS AND COMPOUNDS

www.elsevier.com/locate/jallcom

Microstructure and optical properties of nanocrystalline $CaWO_4$ thin films deposited by pulsed laser ablation in room temperature

Jeong Ho Ryu [a,b,*], Sin Young Bang [b], Woo Sik Kim [b], Gyeong Seon Park [b], Kang Min Kim [b], Jong-Won Yoon [b], Kwang Bo Shim [b], Naoto Koshizaki [c]

[a] *Electro Materials & Device Laboratory, Cooperate R&D Institute, Samsung Electro-Mechanics Co., Ltd., 314, Maetan3-Dong, Yeongtong-Gu, Suwon City, Gyunggi-Do 443-743, South Korea*

[b] *Department of Ceramic Engineering, Ceramic Processing Research Center (CPRC), Hanyang University, 17 Haengdang-Dong, Seongdong-Gu, Seoul 133-791, South Korea*

[c] *Nanoarchitectonics Research Center (NARC), National Institute of Advanced Industrial Science and Technology (AIST), Central 5 1-1-1 Higashi, Tsukuba, Ibaraki 305-8565, Japan*

Received 17 January 2006; accepted 4 July 2006

Available online 30 October 2006

Abstract

Nanocrystalline $CaWO_4$ films were successfully deposited by pulsed laser ablation at various background Ar gas pressures (10–100 Pa) without substrate heating or after annealing treatment. The effects of Ar pressure on microstructure, surface morphology, chemical composition and optical properties were investigated by XRD, HR-TEM, FE-SEM, XPS, UV–vis and PL analyses. The crystallite size of $CaWO_4$ films increased with increasing Ar pressure, which was associated with a change of surface morphology. Reduced tungsten states [W^{5+}] or [W^{4+}] caused by oxygen vacancies were observed at 10 Pa. However, over 50 Pa, the atomic concentration of all the constituent elements was almost constant, especially [Ca]/[W] ratio, which was nearly unity. The optical energy band-gap of $CaWO_4$ films was strongly dependent on the Ar pressure, i.e., decreased from 4.9 to 4.5 eV with the increase of Ar pressure from 50 to 100 Pa. The photoluminescence (PL) spectra was positioned in a blue-shifted region around 378 nm compared with emission at 420 nm of bulk $CaWO_4$ target, which clearly demonstrates the optical band-gap widening phenomena induced by quantum-size effect.

Keywords: Oxide materials; Thin films; Laser processing; Microstructure; Luminescence

1. Introduction

The synthesis and electro-optical properties of scheelite-type metal tungstates have been intensively investigated during the past half century [1–20]. Especially, calcium tungstate ($CaWO_4$) has attracted particular attention because it has been found to have practical importance as MASER materials [4–6] and scintillators [7,8] in quantum electronics and medical applications. The $CaWO_4$ single crystals and polycrystalline powder have been prepared by several techniques such as the Czochralski method [9,10], precipitation route [11,12], hydrothermal synthesis [13] and solid-state reactions [14,15]. It is generally agreed that a thin film phosphor has superior resolution compared to powder because of inherently smaller grain size and less lateral scattering. Various physical and chemical deposition methods including sputtering deposition [16], vacuum evaporation [17], electron beam evaporation [18], electrochemical route [19] and spray pyrolysis [20] have been reported for preparation of the $CaWO_4$ films.

However, $CaWO_4$ films prepared by the sputtering contain Ca_3WO_6, Ca_6WO_9 and WO_3 as impurity phases induced by high vapor pressure of WO_3 [16]. Moreover, $CaWO_4$ films prepared by vacuum evaporation showed no luminescence because of poor crystallinity [17] unless subjected to heat treatment (500–1100 °C), which led to cracking and/or peeling of the films. Such problems have rendered preparation of the $CaWO_4$ films difficult.

---

[*] Corresponding author at: Electro Materials & Device Laboratory, Cooperate R&D Institute, Samsung Electro-Mechanics Co., Ltd., 314, Maetan 3-Dong, Yeongtong-Gu, Suwon-City,Gyunggi-Do 443-743, South Korea.
Tel: +82 31 210 3089; Fax: +82 31 300 7900.
E-mail address: jimihen.ryu@samsung.com (J.H. Ryu).

0925-8388/$ – see front matter © 2006 Elsevier B.V. All rights reserved.
doi:10.1016/j.jallcom.2006.07.130

Recently, extensive and successful efforts on pulsed laser ablation (PLA) have been undertaken and successfully employed in the past for thin film processing [21–24], since it is a powerful and attractive choice for preparation of stoichiometric high-quality complex compound films. The excellent capability of the PLA for reactive deposition and to transfer the original stoichiometry of bulk targets to the deposited film makes it suitable for the fabrication of simple and complex oxide films [25–27]. Therefore, it is interesting challenge to synthesize thin films of scheelite-type complex oxides by using PLA technique. Tanaka et al. [28] reported film fabrication of $CaWO_4$ by PLA using targets composed of CaO and WO_3 mixtures. However, no crystalline $CaWO_4$ film was obtained in their conditions at substrate temperature below 600 °C [28].

In this study, we report deposition and characterization of nanocrystalline $CaWO_4$ films using PLA without substrate heating or after-annealing treatment. Improved understanding of the relationship between growth conditions, microstructures and physical properties are essential to produce the film to meet the requirements of a given technological application, because the properties and application of the resulting $CaWO_4$ films are sensitive to the growth conditions employed in the film deposition. For these reasons, we focused our attention on the room temperature growing mechanism in PLA process and effects of background Ar pressure on the microstructure and optical properties. Moreover, this allowed us to investigate the quantum-size effect on optical energy band-gap and photoluminescence (PL) emission of the $CaWO_4$ films.

2. Experimental

The polycrystalline $CaWO_4$ powder was prepared by solid-state reaction method. At first, 50 mL of ethanol (99.5%) was added to a stoichiometric mixture of $CaCO_3$ (purity 99.99%, Wako Chemical Co. Ltd., Japan) and H_2WO_4 (purity 99.99%, High Purity Chemical Co. Ltd., Japan), and subsequently mixed in a planetary ball-mill for 12 h. The resultant mixture was then filtered, dried and reacted in 800 °C for 5 h in an alumina crucible and then cooled down to room temperature. The heat-treated powder was uni-axially cold-pressed into a disk-shaped pellet with 300 MPa and then sintered at 1000 °C for 3 h in an oxygen atmosphere. The resulting polycrystalline target was white–yellow in color and powder XRD measurement indicated that the target was single phase and consistent with JCPDS data (card number, 41-1431) as shown in Fig. 1(a).

An Nd-YAG laser (wavelength = 355 nm) was used for the ablation. The repetition rate and pulse width of the laser were 10 Hz and 7 ns, respectively. The quartz substrate, with typical sizes of 10 mm × 20 mm × 1 mm, was first ultrasonically cleaned in acetone and then mounted near the target at an off-axial position in order to minimize the concentration of undesirable particles and outgrowths on the film surface [29–31]. The laser beam was focused through an optical window at a 45° oblique incidence onto the target, which was rotating at a rate of 30 rpm to avoid drilling. The maximum laser energy was set at 200 mJ/pulse and total irradiation pulses were approximately 20,000. The base pressure prior to laser ablation was about 1×10^{-7} Torr and working pressure of background Ar gas was varied in a range from 10 to 100 Pa. All deposition processes were carried out in room temperature without substrate heating.

The crystallinity and microstructure were examined by an X-ray diffractometer (XRD, Rigaku RAD-C, Japan) using Cu Kα radiation and a high resolution transmission electron microscope (HR-TEM, JEOL 4010, Japan) equipped with a field emission gun operating at 400 kV. Surface morphology was observed using field-emission scanning electron microscope (FE-SEM, Hitachi, S-4800). The surface composition and chemical states analyses were performed with X-ray photoelectron spectroscopy (XPS, PHI 5600ci, USA) using a monochromated Al Kα source (1486.5 eV, 100 W). The typical pass energy and the energy resolution were 5.85 eV and 0.05 eV/step, respectively. The binding energy values were calibrated with the C 1s line of adventitious carbon at 284.5 eV. Optical absorption property was measured with a UV–vis spectrophotometer (Shimadzu, UV-2100PC, Japan) and room temperature PL spectra were recorded with a luminescence spectrophotometer (PerkinElmer, LS45, USA) using quasi-monochromatic light dispersed by a 0.5 monochromator from a xenon lamp as optical excitation source.

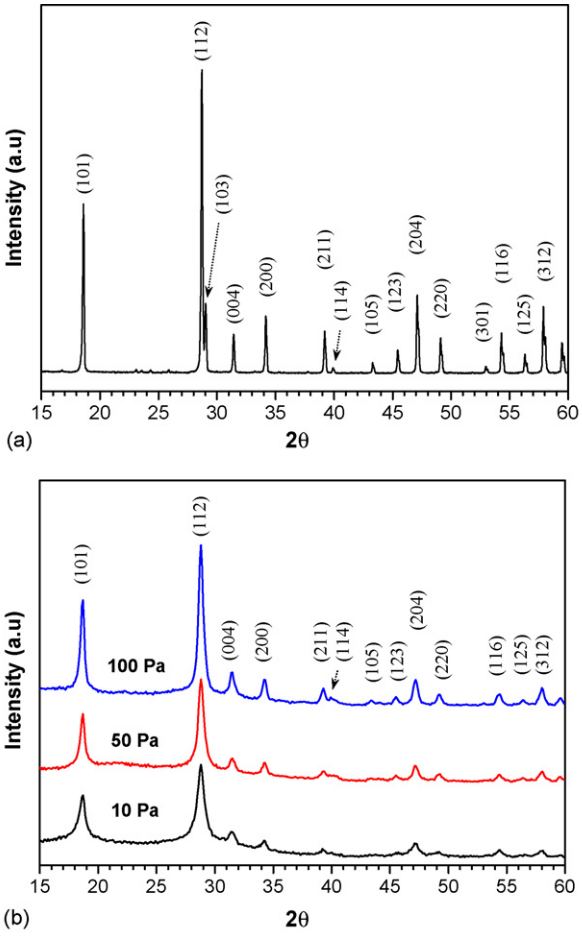

Fig. 1. XRD patterns of: (a) bulk target and (b) nanocrystalline $CaWO_4$ films deposited at various Ar pressures.

3. Results and discussion

The X-ray diffraction patterns of the bulk target and nanocrystalline $CaWO_4$ films deposited under various Ar pressures are presented in Fig. 1. $CaWO_4$ crystals exist in nature as scheelite-type tetragonal structure. In the scheelite structure, [W]-ions are in tetragonal [O]-ion cages and isolated from each other, and [Ca]-ion is surrounded by eight oxygen ions [32]. At all Ar pressures in Fig. 1(b), most of the prominent peaks corresponding scheelite-type $CaWO_4$ phase were clearly observed without any un-reacted or additional phases such as CaO, WO_3, Ca_2WO_6 or Ca_6WO_9 phases. By increasing Ar pressure from 10 to 100 Pa, intensity of XRD peaks increased and full width at half maximum decreased, indicating that crystallinity and crystallite size increased. The particle sizes were calculated from (1 1 2) peaks using Scherrer's formula. $D = k\lambda/\beta\cos\theta$, where D is the average grain size, k a constant equal to 0.89, λ the wavelength of X-rays and β is the corrected half-width that is obtained by using (1 1 1) line of the pure silicon as the standard. The calculated average crystallite sizes of $CaWO_4$ were 8.2, 10.9, and 13.6 nm at Ar pressures of 10, 50, 100 Pa, respectively.

Fig. 2(a) through (c) present high-resolution transmission electron microscope (HR-TEM) images of the nanocrystalline $CaWO_4$ films deposited in various Ar pressures. From the electron diffraction patterns, several groups of diffraction rings are identified and indexed in inset of Fig. 2(c). The electron diffraction rings correspond well with d spacing of scheelite-type $CaWO_4$. Mean particle sizes of $CaWO_4$, calculated from about 100 particles in the TEM images, were 8.5 nm for films deposited at 10 Pa, 11.3 nm at 50 Pa and 13.8 nm at 100 Pa. This agrees well with the results calculated by XRD.

Fig. 3(a–c) represents surface morphology of the nanocrystalline $CaWO_4$ films deposited at various Ar pressures. The surface of the $CaWO_4$ film deposited at 10 Pa was smooth. However, at higher Ar pressures, the surface became rougher resulting from the formation of nanometer-sized particulates. This change in the surface morphology can be attributed to the collision phenomena in the PLA process [33]. Low ambient pressures allow the ejected species to land on the substrate for continuous film formation. However, the plume confined by high ambient pressures induces multiple collisions, and thereby the super-saturation and condensation of the vaporized materials in the ambient gas take place. As a result, larger particulates are deposited on the substrate at Ar pressure of 100 Pa. According to our previous report on preparation of perovskite oxides using PLA in room temperature, the particle size and surface roughness of nanocrystalline $BaTiO_3$ and $LaFeO_3$ increased with increasing Ar pressure in a pressure range of 10–100 Pa [33]. Therefore, it is considered that the growing mechanism of nanocrystalline $CaWO_4$ at different Ar pressures in room temperature is similar to those of the perovskite oxides.

The XPS was used to infer the influence of the Ar pressure on the chemical composition of the $CaWO_4$ films. Fig. 4(a and b) shows the high-resolution XPS spectra of the [Ca] 2p and [W] 4f regions of the $CaWO_4$ films deposited in a range from 10 to 100 Pa. The measured binding energies and branching ratio of the [Ca] $2p_{1/2}$ and $2p_{3/2}$ spin–orbit doublet at 350.4 and 346.8 eV are typical values of oxidized states of the [Ca] [34,35]. The [W] 4f core level spectrum recorded on samples at 50 and 100 Pa shows the two components associated with $4f_{5/2}$ and $4f_{7/2}$ spin–orbit doublet at 37.5 and 35.4 eV, respectively. These values are in agreement with those found in the literature for [W^{6+}] in stoichiometric films [34–36]. However, the spectrum of the sample deposited at 10 Pa have another peak shifted towards lower binding energy, which may be caused by the contribution of [W^{5+}] or [W^{4+}] states resulting from oxygen vacancies in the films [37]. It was reported that these states could play an important role in the transmittance as defect centers [38].

The atomic ratio of [Ca]/[W] estimated from XPS is presented in inset of Fig. 4(b). From the XPS analysis of the films, oxygen deficiency was observed and the [Ca] ion was rich compared to the [W] ion at the low-pressure range of 10 Pa. However, over 50 Pa, atomic concentration of all constituent elements was almost constant, especially the [Ca]/[W] ratio, which was almost unity. When density and energy of the ablated particles are not very high, interaction of plume with background gas can be considered as the scattering of a molecular beam by the particles of

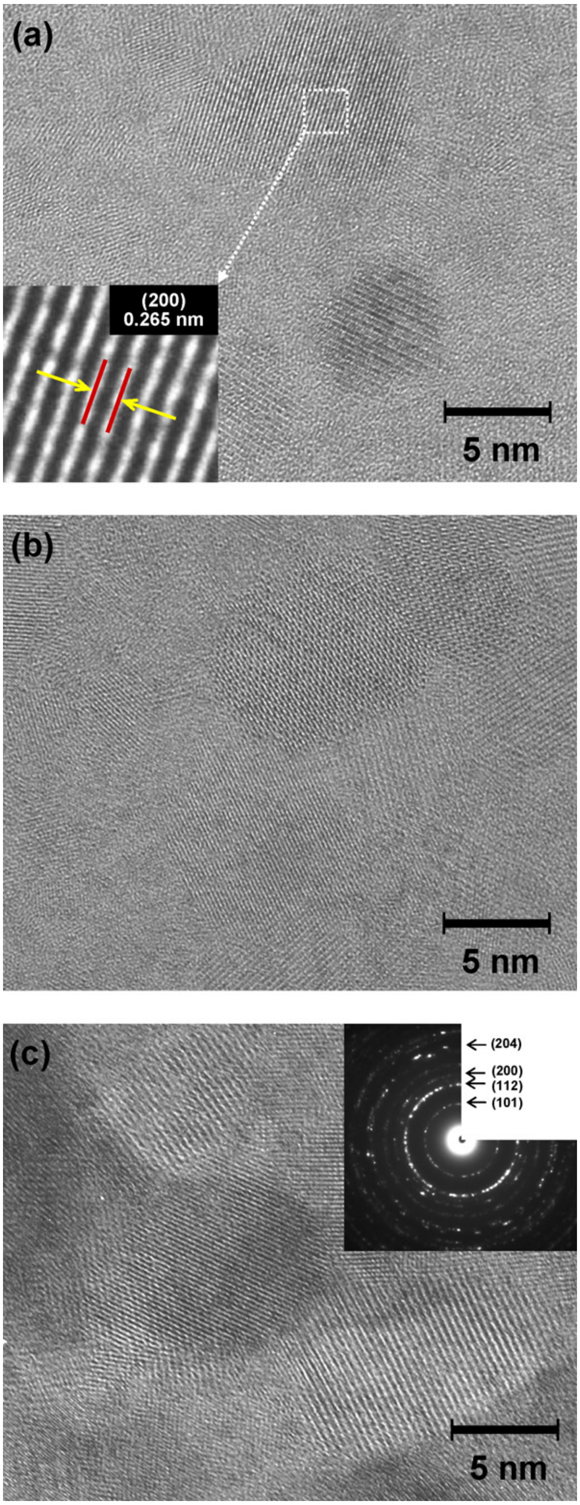

Fig. 2. HR-TEM images of nanocrystalline $CaWO_4$ films deposited on carbon film at: (a) 10 Pa, (b) 50 Pa and (c) 100 Pa. The selected area electron diffraction patterns corresponding to (c) are shown in inset.

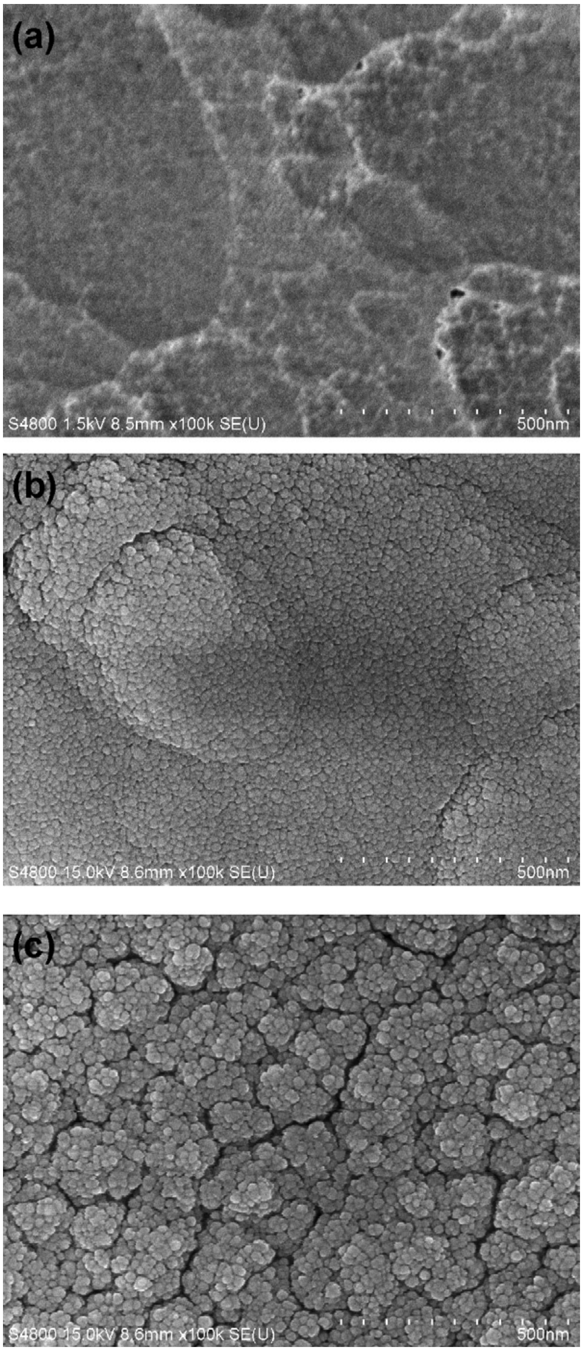

Fig. 3. Surface morphology of nanocrystalline $CaWO_4$ films deposited at: (a) 10 Pa, (b) 50 Pa and (c) 100 Pa. The roughness of the film surfaces increases with the Ar pressure.

the background gas [39,40]. It is well known from a Monte Carlo simulation that non-stoichiometric deposition takes place when target is ablated into ambient gas with low pressure [40]. According to the simulated results, the increase of the background pressure was found to give rise to the more uniform distribution of the deposited particles and the constant stoichiometric ratio. This simulated calculation explains our experimental results on the stoichiometric variation in $CaWO_4$ films well.

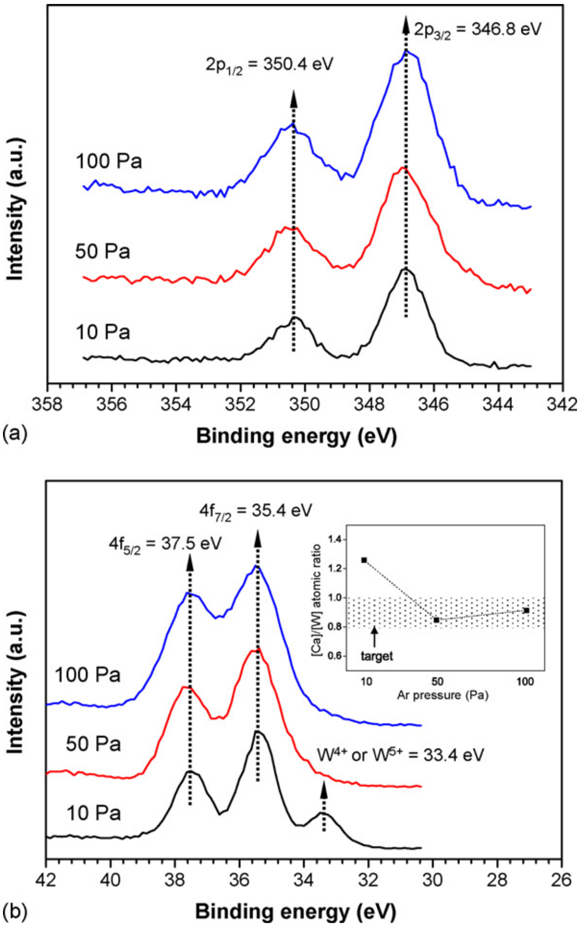

Fig. 4. XPS spectra of the: (a) [Ca] 2p energy region and (b) [W] 4f energy region of the $CaWO_4$ films deposited at various Ar pressures. The [Ca]/[W] atomic ratio of the films is shown in inset of (b).

The optical absorption spectra of the nanocrystalline $CaWO_4$ films deposited at various Ar pressures are presented in inset of Fig. 5. The absorption spectra of $CaWO_4$ films deposited at 50 and 100 Pa showed a typical absorption edge around 280 and 310 nm, respectively. The fundamental absorption mechanism of $CaWO_4$ is attributed to charge-transfer transition in which an oxygen 2p electron goes into on of the empty tungsten

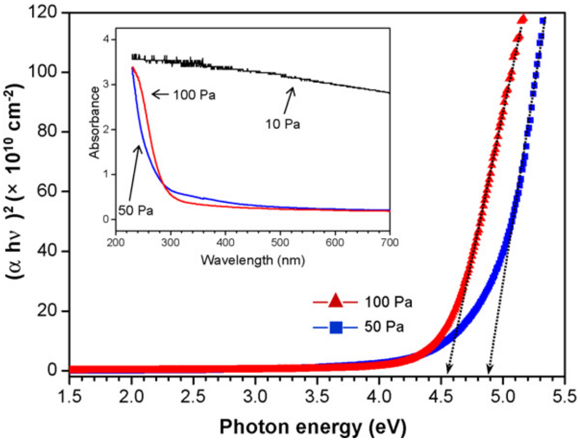

Fig. 5. Optical absorption spectra of nanocrystalline $CaWO_4$ thin films deposited at 50 and 100 Pa (inset) and plots of $(\alpha h\nu)$ vs. $(h\nu)$. The optical energy band-gap is deduced form the extrapolation of the straight line up to $(\alpha h\nu)^2 = 0$.

5d orbitals, i.e., the transitions between $^1A_1$ ground state and $^1T_2$ excited state within [WO_4^{2-}] complex [1–3]. The abnormal flat absorption curve in 10 Pa can be explained by surface scattering effect in oxygen defect sites, which was investigated in XPS analysis. The optical energy band-gap, E_{gap}, for the nanocrystalline $CaWO_4$ films were determined form the sharply increasing absorption region. According to Tauc and Menth's law [41], the absorption coefficient has the following energy dependence, $\alpha(h\nu) = A(h\nu - E_{gap})^m$, where A is a proportionality constant, m another constant, which is different for the transition types ($m = 1/2$, 2, 3/2 or 3 for allowed direct, allowed indirect, forbidden direct and forbidden indirect electronic transitions, respectively), $h\nu$ is photon energy, and E_{gap} is the Tauc optical energy band-gap. The plots of $(\alpha h\nu)^2$ versus photon energy ($h\nu$) for the $CaWO_4$ nanocrystalline films deposited at various Ar pressures are displayed in Fig. 5. In low energy region of the edge, the absorption spectrum deviated from the straight line plot. However, in high energy region of the absorption edge, $(\alpha h\nu)^2$ varied linearly with photon energy ($h\nu$). This straight line behavior in the high energy region was taken as prime evidence for the direct band-gap. The optical band-gap was therefore determined by extrapolating the linear portion of the plot relating $(\alpha h\nu)^2$ versus $h\nu$ to $(\alpha h\nu)^2 = 0$ (see Fig. 5). The optical energy band-gap was estimated to be about 4.9 and 4.5 eV for films deposited at 50 and 100 Pa, respectively. It was reported that $CaWO_4$ has direct band-gap of 4.09 eV in Γ direction calculated by using the linearized-augmented-plane-wave method [42]. The band-gap widening of nanocrystalline $CaWO_4$ films compared to the simulated theoretical values (4.09 eV) is considered mainly due to quantum-size effects. It is clear that the optical energy band-gap is higher for films deposited at 50 Pa, where the grain size is relatively lower than that of 100 Pa. When the average crystal dimension becomes small, the quantum-size effect results in widening of the optical band-gap. The widening of optical energy band-gap with reduction in size was also reported for several other complex oxide films [43–45].

The room temperature photoluminescence (PL) emission spectra of the $CaWO_4$ films deposited at Ar pressure of 50 and 100 Pa are shown in Fig. 6(a and b). The PL emission spectra of the $CaWO_4$ films were obtained at excitation of 240 nm. It is well known that $CaWO_4$ shows emission in the blue or green regions depending on excitation wavelength or energy. Especially, optical band-edge excitation yields a strong blue emission and near-band-edge excitation yields a green emission. Most of the studies on room temperature PL for $CaWO_4$ crystals reported a blue emission around 420 nm for excitation between 240 and 280 nm and a green emission around 510 and 540 nm for excitation between 300 and 315 nm [1–8]. For the $CaWO_4$ films prepared by electron beam evaporation [18], electrochemical method [19] and PLA of oxide mixtures in high temperature [28], only blue emissions at 420–460 nm were obtained at room temperature.

Consisted with the optical band-gap widening estimated from the Tauc plot in Fig. 5, both nanocrystalline $CaWO_4$ films deposited 50 and 100 Pa exhibited a sharp blue emission peak near 378 nm. For comparison, a PL spectrum of the bulk $CaWO_4$ target is shown together in inset of Fig. 6(a). It is noted that the nanocrystalline $CaWO_4$ films deposited by PLA have blue shifted PL emission spectra about 40 nm compared to bulk target at room temperature. This blue shift of PL spectra and band-gap widening at the films with relatively small grain size may be considered mainly due to the quantum-size effect. In the films prepared at 50 and 100 Pa as shown in Figs. 2 and 3, there exist very small nanocrystallites, grain boundaries and imperfections, which lead to larger free carrier concentrations and the existence of potential barriers at the boundaries. Therefore, electric fields are formed and this results in band-gap widening. In particular, the film deposited at 50 Pa had two Gaussian components shifted to higher energy range shown in Fig. 6(a), which are attributed to the presence of smaller nanocrystallites. Moreover, there was another Gaussian component in a lower energy range for the film deposited at 100 Pa as shown in Fig. 6(b), which shows that the PL spectra shifted to a lower energy range with an increase of particle size. It is very clear that the optical energy band-gap is much wider for films deposited at lower Ar pressures, where the crystallite size is relatively smaller than that of higher Ar pressures.

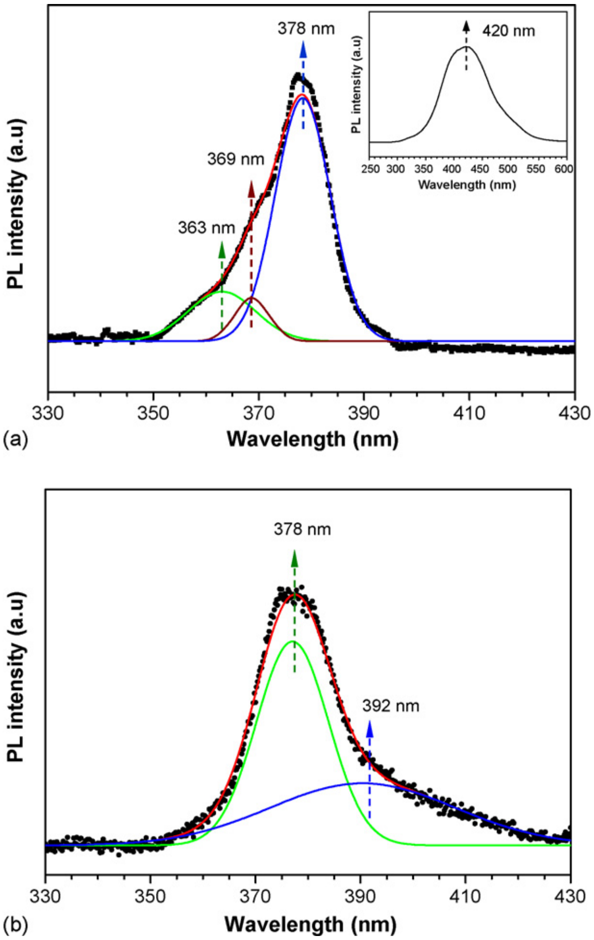

Fig. 6. PL emission spectra of the $CaWO_4$ films deposited at: (a) 50 Pa and (b) 100 Pa. The decomposed Gaussian curves are given with PL spectrum. The inset shows the room temperature PL spectrum of the bulk target for comparison with nanocrystalline films.

4. Conclusions

Nanocrystalline $CaWO_4$ films were successfully deposited by PLA in room temperature with controlling the Ar pressures from 10 to 100 Pa. The films had a single scheelite phase with an average crystallite size around 10 nm. The crystallite size and surface roughness tended to increase with Ar pressure, which was due to the formation of nanoparticulates. The Ar gas pressure was found to influence the stoichiometric ratio of the films and the [Ca]/[W] ratio was close to unity at Ar pressure above 50 Pa, which ascertained that the increase of Ar pressure resulted in uniform stoichiometrical ratio of the films. The estimated optical band-gap of nanocrystalline $CaWO_4$ films deposited at 50 Pa was estimated to 4.9 eV and decreased to 4.5 eV with the increase of Ar pressure to 100 Pa. The optical band-gap widening and blue-shift of PL spectra of the $CaWO_4$ nanocrystalline films compared with bulk target was attributed mainly to the quantum-size effect induced by very small crystallite size. It is worthy to note that this is the new approach for room temperature deposition of nanocrystalline $CaWO_4$ films using PLA. Furthermore, the experimental evidence for the optical band-gap widening and blue-shift of PL emission spectra can be helpful for understanding the quantum-size effect on the band-structure of metal tungstates.

Acknowledgement

This work was supported by the Korea Science and Engineering Foundation (KOSEF) through the Ceramic Processing Research Center (CPRC).

References

[1] R. Grasser, A. Scharmann, K.-R. Strack, J. Luminesc. 27 (1982) 263–272.
[2] M.J. Treadaway, R.C. Powell, J. Chem. Phys. 61 (1974) 4003–4011.
[3] G. Born, A. Hofstaetter, A. Scharmann, G. Schwarz, J. Luminesc. 1/2 (1970) 641–650.
[4] A. Yariv, S.P.S. Porto, K. Nassau, J. Appl. Phys. 33 (1962) 2519–2521.
[5] L.F. Johnson, G.D. Boyd, K. Nassau, R.R. Soden, Phys. Rev. 126 (1962) 1406–1409.
[6] L.F. Johnson, R.A. Thomas, Phys. Rev. 131 (1963) 2038–2040.
[7] J.W. Coltman, E.G. Ebbighausen, W. Altar, J. Appl. Phys. 18 (1947) 530–544.
[8] D.R. Shearer, L.E. Rowe, Med. Phys. 14 (1987) 197–201.
[9] A.R. Chaudhuri, L.E. Phaneuf, J. Appl. Phys. 34 (1963) 2162–2167.
[10] C.D. Brandle, J. Cryst. Growth 264 (2004) 593–604.
[11] A. Sen, P. Pramanik, J. Eur. Ceram. Soc. 21 (2001) 745–750.
[12] V. Thangadurai, C. Knittlmayer, W. Weppner, Mater. Sci. Eng. B 106 (2004) 228–233.
[13] J.T. Kloprogge, M.L. Weier, L.V. Duong, R.L. Frost, Mater. Chem. Phys. 88 (2004) 438–443.
[14] G. Bayer, H.-G. Wiedemann, Thermochim. Acta 133 (1988) 125–130.
[15] R.B. Pode, S.J. Dhoble, Phys. Status Solidi B 203 (1997) 571–577.
[16] Y. Kashiwakura, O. Kanehisa, Japanese Patent No. 1-263188 (1989).
[17] C. Feldman, J. Soc. Motion Pict. Eng. 67 (1958) 455–460.
[18] P.F. Carcia, M. Reilly, C.C. Torardi, M.K. Crawford, C.R. Miao, B.D. Jons, J. Mater. Res. 12 (1997) 1385–1390.
[19] W.-S. Cho, M. Yashima, M. Kakihana, A. Kudo, T. Sakata, M. Yoshimura, Appl. Phys. Lett. 66 (1995) 1027–1029.
[20] Z. Lou, M. Cocivera, Mater. Res. Bull. 37 (2002) 1573–1582.
[21] J.-G. Zhang, J.M. McGraw, J. Turner, D. Ginley, J. Electrochem. Soc. 144 (1997) 1630–1634.
[22] S.H. Shim, K.B. Shim, J.-W. Yoon, Y. Shimizu, T. Sasaki, N. Koshizaki, Thin Solid Films 472 (2005) 11–15.
[23] G.J. Fang, K.-L. Yao, Z.-L. Liu, Thin Solid Films 394 (2001) 64–71.
[24] D.G. Chrisey, G.K. Huber, Pulsed Laser Deposition of Thin Films, Wiley Publications, New York, 1994.
[25] V.F. Vratskikh, Y.N. Drozdov, V.V. Talanov, Supercond. Sci. Technol. 10 (1997) 766–768.
[26] H. Fan, S.A. Reid, Chem. Mater. 15 (2003) 564–567.
[27] C.V. Ramana, O.M. Hussain, R. Pinto, C.M. Julien, Appl. Surf. Sci. 207 (2003) 135–138.
[28] K. Tanaka, K. Fukui, K. Ohga, C.K. Choo, J. Vac. Sci. Technol. A 20 (2002) 486–491.
[29] B. Holzapfel, B. Roas, L. Schults, P. Bauer, G.S. Ischenko, Appl. Phys. Lett. 61 (1992) 3178–3180.
[30] Z. Trajanovic, L. Senapati, R.P. Sharma, T. Venkatesan, Appl. Phys. Lett. 66 (1995) 2418–2420.
[31] Y. Zhao, M. Ionescu, J. Horvat, S.X. Dou, Supercond. Sci. Technol. 18 (2005) 395–399.
[32] L. Bragg, G.F. Claringbull, Crsytal Structures of Minerals, G. Bell and Sons Ltd., London, 1965.
[33] J.W. Yoon, T. Sasaki, N. Koshizaki, Appl. Phys. A 76 (2003) 641–643.
[34] J.F. Mlulder, W.F. Stickle, P.E. Sobol, K.D. Bomben, Handbook of X-ray Photoelectron Spectroscopy, Perkin-Elmer, Eden Prairie, MN, 1992.
[35] N. Alarcón, X. García, M.A. centeno, P. Ruiz, A. Gordon, Appl. Catal. A 267 (2004) 251–265.
[36] J.E. Germain, in: M. Che, G.C. Bond (Eds.), Adsorption and Catalysis on Oxide Surfaces, Elsevier, Amsterdam, 1985, p. 335.
[37] L. Ottaviano, F. Bussolotti, L. Lozzi, M. Passacantando, S.L. Rosa, S. Santucci, Thin Solid Films 436 (2003) 9–16.
[38] G. Leftheriotis, S. Papaefthimiou, P. Yianoulis, A. Siokou, Thin Solid Films 384 (2001) 298–306.
[39] D.J. Lichtenwalner, O. Auciello, R. Dat, A.I. Kingon, J. Appl. Phys. 74 (1993) 7497–7505.
[40] T.E. Itina, W. Marine, M. Autric, J. Appl. Phys. 82 (1997) 3536–3542.
[41] J. Tauc, A. Menth, J. Non-Cryst. Solids 8/9 (1972) 569–585.
[42] Y. Zhang, N.A.W. Holzwarth, R.T. Williams, Phys. Rev. B 57 (1998) 12738–12750.
[43] X.M. Lu, J.S. Zhu, W.Y. Zhang, G.Q. Ma, Y.N. Wang, Thin Solid Films 274 (1996) 165–168.
[44] G. Pang, S. Chen, Y. Zhu, O. Palchik, Y. Koltypin, A. Zaban, A. Gedanken, J. Phys. Chem. B 105 (2001) 4647–4652.
[45] X.G. Tang, H.R. Zeng, A.L. Ding, P.S. Qiu, W.G. Luo, H.Q. Li, D. Mo, Solid State Commun. 116 (2000) 507–511.